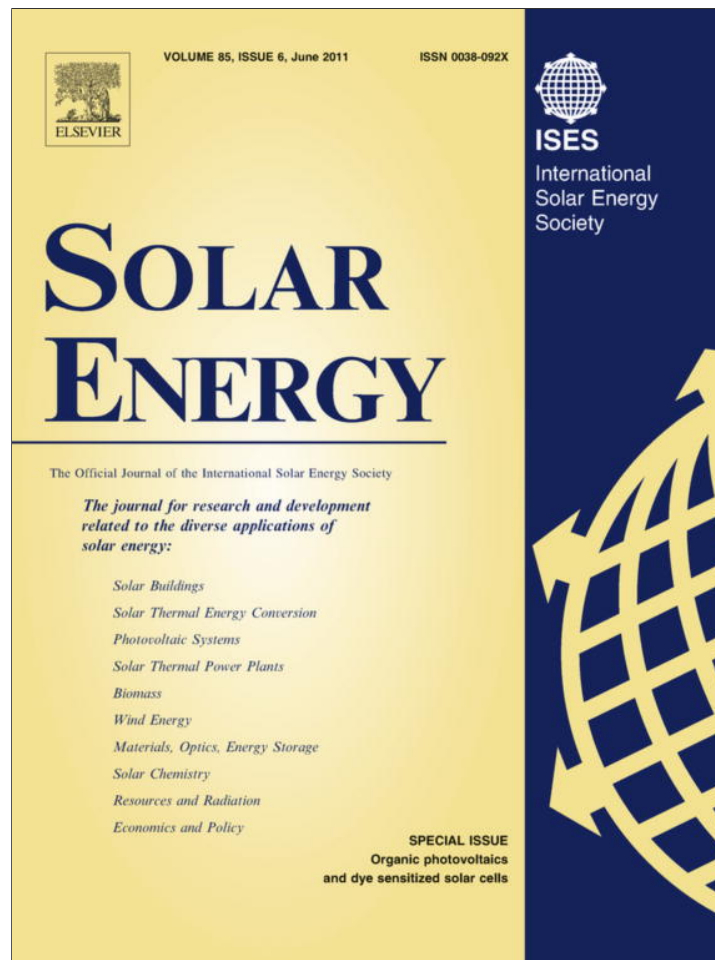


Provided for non-commercial research and education use.
Not for reproduction, distribution or commercial use.



This article appeared in a journal published by Elsevier. The attached copy is furnished to the author for internal non-commercial research and education use, including for instruction at the authors institution and sharing with colleagues.

Other uses, including reproduction and distribution, or selling or licensing copies, or posting to personal, institutional or third party websites are prohibited.

In most cases authors are permitted to post their version of the article (e.g. in Word or Tex form) to their personal website or institutional repository. Authors requiring further information regarding Elsevier's archiving and manuscript policies are encouraged to visit:

<http://www.elsevier.com/copyright>



Charge extraction with linearly increasing voltage: A numerical model for parameter extraction

M.T. Neukom^{a,*}, N.A. Reinke^{a,1}, B. Ruhstaller^{a,b}

^a *Institute of Computational Physics, ZHAW, Zurich University of Applied Sciences, Technikumstr. 9, 8401 Winterthur, Switzerland*

^b *Fluxim AG, Dorfstrasse 7, 8835 Feusisberg, Switzerland*

Available online 29 April 2011

Communicated by: Associate Editor Hari Upadhyaya

Abstract

An accurate determination of the charge carrier mobilities is essential to model and improve organic solar cells. A frequently used method to determine charge carrier mobilities is the charge extraction by linearly increasing voltage technique (CELIV). In this technique a voltage ramp is applied to the device in order to extract free charge carriers inside the bulk. The free charge carriers can be created by injection or by a short light flash (photo-CELIV). With a simple analytical formula the mobility is commonly estimated on the basis of the temporal position of the current peak.

We simulate the photo-CELIV experiment with a fully-coupled electro-optical model to analyse the accuracy and limitations of the analytical formulas that are used to calculate the mobilities. We show that for thin film solar cells RC-effects are problematic and can lead to inaccurate results. If RC-effects are negligible only the order of magnitude of the fast carrier mobility can be determined using the analytical formula. We measure CELIV currents for several voltage slopes and transient photo-currents of an organic bulk heterojunction solar cell. By fitting our numerical model to the multiple curves we show that important material parameters like the electron mobility, hole mobility, charge generation and recombination efficiency can be determined using numerical parameter extraction.

Crown Copyright © 2011 Published by Elsevier Ltd. All rights reserved.

Keywords: CELIV; Charge carrier mobility; Numerical simulation; Parameter extraction; Drift-diffusion

1. Introduction

Record solar power conversion efficiencies up to 8.1 % (Solamer, 2010) for organic solar cells are encouraging but still too low for large scale energy production. To further improve the efficiency and also the lifetime of organic solar cells it is essential to understand the device physics and to both identify and quantify the limiting factors. Measuring current–voltage-characteristics is restricted to the determination of performance parameters like the power conversion efficiency and the fill factor and thus gives only a limited insight into the underlying physical processes.

More fundamental physical parameters including charge carrier mobilities and recombination efficiency become accessible by transient measurement techniques. One of these dynamic measurement techniques is charge extraction with linearly increasing voltage (CELIV) and is frequently used to determine mobilities of organic and inorganic solar cells.

In order to measure charge carrier mobilities, the CELIV technique has some significant advantages compared with other known techniques. For time-of-flight (TOF) (Mark and Lampert, 1970; Mort and Pai, 1976) measurements a special sample preparation is needed. TOF is only possible with thick layers (above 2 μm) which is not feasible for spin-coated organic materials. CELIV can be done with regular solar cells. An other well-known technique is the steady-state, trap-free, space-charge limited current method (TF-SCLC) and the dark injection

* Corresponding author. Tel.: +41 0 58 934 74 88.

E-mail addresses: martin.neukom@zhaw.ch (M.T. Neukom), nils.reinke@zhaw.ch (N.A. Reinke).

¹ Tel.: +41 0 58 934 77 98.

space-charge limited transient current method (DI-SCLC) (Mark and Lampert, 1970). Both techniques can only be used for unipolar devices whereas CELIV can extract the faster charge carrier mobility in bipolar devices.

In the CELIV experiment free charge carriers that are inside the device are extracted with a linearly increasing voltage. The free charge carriers are either equilibrium carriers (due to doping or impurities), the charge carriers are injected by the electrodes or they are generated by a light pulse typically performed with a short laser flash.

Due to the linearly changing voltage a constant displacement current occurs due to the capacitance of the cell. The charge carriers that are extracted lead to an additional current that peaks at a characteristic time t_{max} . With the peak-time t_{max} , the thickness of the sample d and the voltage slope A the mobility of the faster carrier μ can be calculated according to Juska et al. (2000, 2001).

$$\mu = \frac{2 \cdot d^2}{3 \cdot A \cdot t_{max}^2} \cdot \frac{1}{\left(1 + 0.36 \cdot \frac{\Delta j}{j(0)}\right)} \quad (1)$$

The factor $1 + 0.36 \cdot \Delta j / j(0)$ is an empirical correction for the redistribution of the electric field where $j(0)$ is the displacement current offset and Δj is the current overshoot (Juska et al., 2001). The model used to derive the basic equation ($2 \cdot d^2 / (3 \cdot A \cdot t_{max}^2)$) is a simple unipolar drift-only model that assumes perfect extraction and an initially constant charge distribution.

Bange and co-workers recently presented a new correction function for the analytical CELIV expression. In their study a numerical model is used to solve the drift-diffusion equations to derive an empirical correction function depending on Δj and $j(0)$.

Lorrmann et al. (2010) generalised the CELIV theory and presented a parametric equation as a solution for the differential equation that has been derived by Juska et al. (2000). The CELIV formula $2 \cdot d^2 / (3 \cdot A \cdot t_{max}^2)$ is the analytical solution of this differential equation and is derived with the assumption of low conducting materials. In contrast the parametric equation is valid for all conductivities but needs to be evaluated computationally.

All the mentioned techniques to analyse transient CELIV currents follow the same basic assumptions like a spatially constant charge carrier distribution at the beginning. For a more comprehensive description of the physical processes we introduced a fully-coupled, electro-optical, numerical simulation (Neukom et al., 2010). We solved the drift-diffusion equations spatially resolved, calculated the initial distribution of electrons and holes and considered the creation and recombination of charge carriers, the energetic barriers (thermionic injection) and the series resistance in the electric circuit of the measurement.

In this paper we present a method for numerical parameter extraction on the basis of CELIV currents and compare numerical simulation with the analytical approach. The comparison of all different techniques to analyse transient CELIV currents is beyond the scope of this study.

Because all the mentioned analytical approaches are based on the same basic simplifications, its deviation to our comprehensive numerical approach is similar. For the comparison of analytical calculation and numerical simulation we use the most frequently used formula (Eq. (1)).

2. Experimental

The device investigated in this study consists of a layer structure as listed in Table 1. The active layer of the solar cell consists of novel small bandgap p-type polymer PT5DPP (Fig. 1) provided by BASF blended with PCBM70. The samples are fabricated by spin-coating of PEDOT and the active polymer blend on a glass substrate with pre-structured ITO-electrodes. The top electrode is deposited by thermal evaporation in vacuum. For more details about the fabrication see (Offermans et al., 2010). The active area of the solar cell is 0.04 cm^2 .

The voltage ramp used in the CELIV experiment is applied by an arbitrary waveform-generator (Picotest G5100A). The cell is illuminated by a pulsed LED (Kingbright L-7113PBC-Z) with a peak wavelength of 468 nm and driven by a second arbitrary waveform-generator of the same type. The transient current is measured by a 12Ω resistor in combination with a voltage amplifier (Femto HVA-10M-60-B). The transient voltages were measured by a digital storage oscilloscope (Acute DS-1302).

3. Model

In this study we use a fully-coupled opto-electrical model to analyse the experimental photo-current transients. The model described in this chapter is implemented

Table 1
Layer structure of the organic solar cell.

Layer	Thickness	Material
0	Semi- ∞	air
1	2 mm	Glass
2	75 nm	ITO
3	60 nm	PEDOT:PSS
4	90 nm	PP5DPP:PCBM70 (1:2)
5	1 nm	LiF (neglected)
6	100 nm	Aluminium

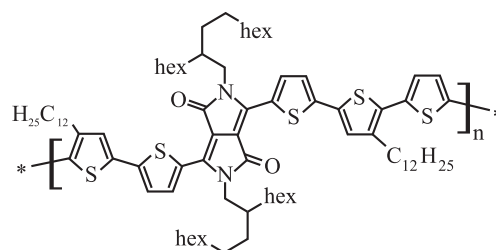


Fig. 1. Chemical structure of PT5DPP (BASF).

in the *semiconducting emissive thin film optical simulator* (SETFOS, www.fluxim.ch).

We calculate the light penetration into the cell with respect to interference effects with a transfer matrix method. The spatially resolved density of absorbed photons per second, derived from the calculated interference pattern, represents a source of charge carriers and is coupled to the electrical model. The formation, diffusion and dissociation of CT-excitons (charge transfer excitons) is neglected since the CT-exciton lifetime is assumed to be much shorter than the time scale of a CELIV experiment (Hwang et al., 2009). Furthermore the widely used model of Onsager–Braun to describe the dissociation process of CT-excitons may not be appropriate for bulk heterofunction solar cells because the orientation of the donor acceptor interface is unknown. Therefore we assume a photon to directly generate an electron–hole pair.

A detailed description of the electro-optical model and its application to steady-state experimental data can be found in our previous publication (Häusermann et al., 2009).

The bulk material acting as active layer is assumed to be one effective medium. A one dimensional spatial discretization with an element size of 1 nm is used to describe the charge transport inside this layer. The relevant equations are

$$\frac{\partial n}{\partial t}(x, t) = \frac{1}{q} \cdot \frac{\partial j_n}{\partial x}(x, t) - R(x, t) + G_{opt} \cdot g(x) \quad (2)$$

$$\frac{\partial p}{\partial t}(x, t) = -\frac{1}{q} \cdot \frac{\partial j_p}{\partial x}(x, t) - R(x, t) + G_{opt} \cdot g(x) \quad (3)$$

$$R(x, t) = \eta \cdot n(x, t) \cdot p(x, t) \cdot (\mu_p + \mu_n) \cdot \frac{q}{\epsilon_r \cdot \epsilon_0} \quad (4)$$

$$j_n(x, t) = n(x, t) \cdot q \cdot \mu_n \cdot E(x, t) + \mu_n \cdot k \cdot T \cdot \frac{\partial n}{\partial x}(x, t) \quad (5)$$

$$j_p(x, t) = p(x, t) \cdot q \cdot \mu_p \cdot E(x, t) + \mu_p \cdot k \cdot T \cdot \frac{\partial p}{\partial x}(x, t) \quad (6)$$

$$\frac{\partial E}{\partial x}(x, t) = -\frac{q}{\epsilon_0 \cdot \epsilon_r} \cdot (p(x, t) - n(x, t)) \quad (7)$$

$$\int E(x, t) \cdot dx = V_{Source} - j_{tot} \cdot S \cdot R_s - \frac{\Phi_A - \Phi_C}{q} \quad (8)$$

$$j_{tot} = j_p(x_1, t) + j_n(x_1, t) + \frac{\partial E}{\partial t}(x_1, t) \cdot \epsilon_r \cdot \epsilon_0 \quad (9)$$

Eq. (2) and (3) are electron (n) and hole (p) continuity equations describing the generation, drift-diffusion and recombination of free charge carriers. For the recombination R of free electrons and holes the Langevin model is used (Eq. (4)). The electron and hole currents are described by the drift-diffusion equations (Eq. (5) and (6)). The electric field E is calculated according the Poisson equation (Eq. (7)).

The series resistance of the experimental set-up has a strong influence on the measured result and can therefore not be neglected in the simulation. The electric circuit with considered R_s used in the simulation is shown in Fig. 2. The effective applied voltage V_{app} at the OSC (organic solar cell)

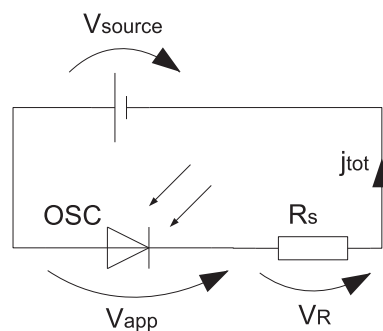


Fig. 2. Sketch of the electrical circuit used in the simulation model.

device is the voltage of the function generator V_{Source} minus the voltage V_R across the series-resistor R_s (cp. Fig. 2). The difference in the work-function of anode Φ_A and cathode Φ_C and the effective applied voltage V_{app} create an electric field inside the active layer (Eq. (8)). The measurable current j_{tot} is the sum of a current due to charge transport and a displacement current (Eq. (9)). The total current j_{tot} is spatially constant at all times.

As a boundary condition we assume thermionic injection to describe the energetic barriers at the electrodes for charge carrier extraction from the cell.

4. Results

In the following two sections we use the analytical formula frequently used to analyse CELIV experiment (Eq. (1)) to analyse the numerically simulated current transients. The mobilities of the simulation (*reference mobilities* μ_{ref}) are then compared with the mobilities calculated with the formula (*apparent mobilities* μ_{app}). This comparison reveals the accuracy and scope of validity of the analytical model. With the CELIV experiment only the faster charge carrier can be determined. Therefore we always compare the apparent mobility with the larger value of the two reference mobilities.

4.1. Influence of RC-effects

In this section the influence of the RC-time of the measurement circuit on the determined CELIV mobilities is analysed. The series resistance of the circuit mainly consists of the internal resistance of the waveform generator and the resistance of the ITO layer and can be up to several 100 Ω . The active layer of an organic solar cell is typically about 100 nm thick leading to a high capacitance. (In our example the device has a capacity of 50 nF/cm².)

In Fig. 3a transient CELIV currents with different series-resistances are shown. A high series resistance leads to a strong shift of t_{max} and to an underestimation of the mobility. The peak is lower with a higher RC-time because charges have more time to disappear by recombination. With lower mobilities the influence of the RC-effects is

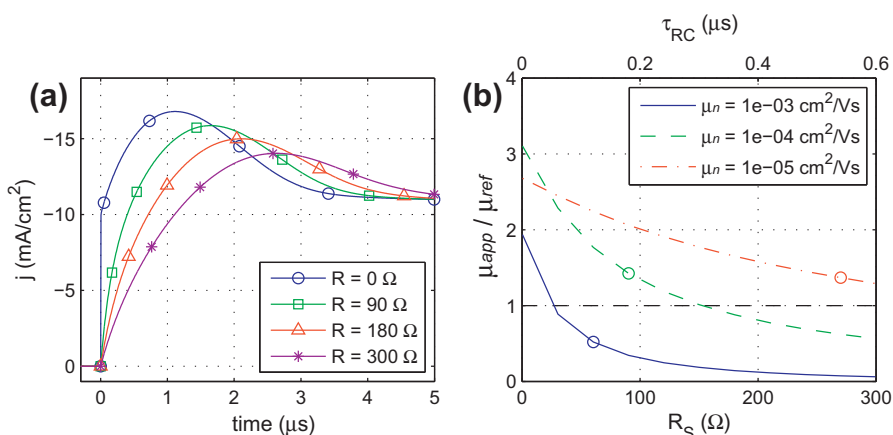


Fig. 3. (a) Simulated CELIV currents with varied series-resistances ($\mu_n = 1 \times 10^{-4} \text{ cm}^2/\text{Vs}$, $\mu_p = 0.01 \times \mu_n$, $A = 0.2 \text{ V}/\mu\text{s}$). (b) Apparent mobilities μ_{app} (calculated with Eq. (1)) relative to the reference mobility μ_{ref} plotted versus the series resistance R_S . The circles mark the point where $t_{max} = 10 \cdot \tau_{RC}$. In this and all subsequent figures we use just a few markers to enhance the visibility. Nevertheless the simulations were done with far beyond 1000 data points.

lower. If the ratio of the peak-time t_{max} to the time constant of the RC-effects τ_{RC} is high the result is more accurate.

The circle in Fig. 3b marks the point where t_{max} is 10 times longer than the RC-time τ_{RC} . The RC-time of a measurement set-up can be estimated (see Eq. (10) and (11)) and the ratio t_{max}/τ_{RC} can be calculated. If this ratio is higher than 10 the apparent mobilities are most likely not underestimated due to RC-effects. In order to keep the ratio high the voltage slope A should be chosen as small as possible because a low voltage slope leads to a longer peak-time t_{max} .

State-of-the-art OSC samples are thin and have a high mobility meaning that analysing CELIV experiments with the analytical formula is problematic for OSC. In this case parameters can be extracted with numerical simulation as shown in chapter Section 4.4.

4.2. Influence of the mobilities

To be able to make conclusions about the accuracy of the analytical CELIV formula (Eq. (1)) we vary several parameters of the simulation and study their influence on the apparent mobilities. In these simulations the RC-effects are disabled by setting $R = 0 \Omega$.

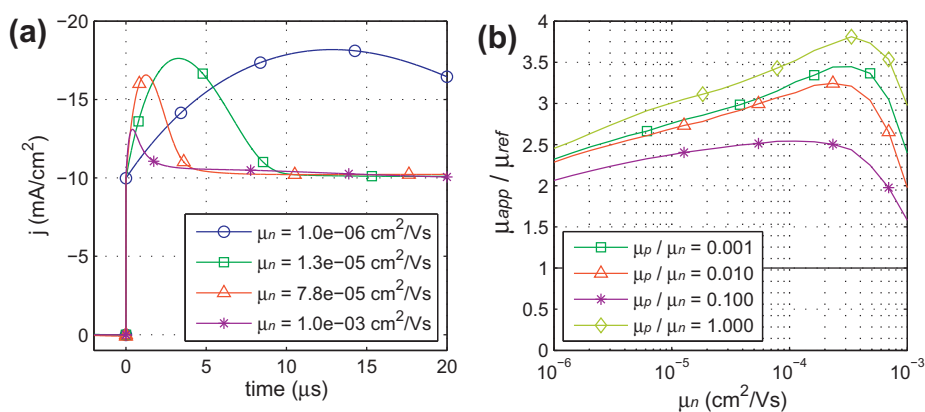


Fig. 4. (a) Simulated CELIV currents with varied electron mobility ($\mu_p = 0.01 \cdot \mu_n$, $A = 0.2 \text{ V}/\mu\text{s}$). (b) Apparent mobilities μ_{app} relative to the reference mobility μ_{ref} plotted versus the reference mobility for several mobility ratios.

The CELIV currents are simulated with different electron mobilities and different mobility ratios. Because the device is symmetric (same injection barriers) the result does not depend on whether the electrons or the holes are the faster carriers. With increasing electron mobility the CELIV-peak shifts to shorter times as shown in Fig. 4a. The current overshoot Δj is lower with a high mobility due to an increased charge carrier recombination. In Fig. 4b the relative apparent mobility is plotted versus the reference mobility. In this case the mobilities are in general overestimated and show a variation by a factor of 1.5–3.5. In the CELIV experiment only the faster charge carrier is analysed. We investigate the influence of the slow charge carrier on the calculated result by using several mobility ratios in Fig. 4b. The results of the apparent mobility can vary up to 100% when varying the slow carrier mobility.

As a conclusion we can state that using the analytical formula only allows to determine the order of magnitude of the mobility. Moreover this is only the case if RC-effects are negligible. Furthermore not only the fast charge carrier but also the slow charge carrier has an influence on the apparent fast carrier mobility.

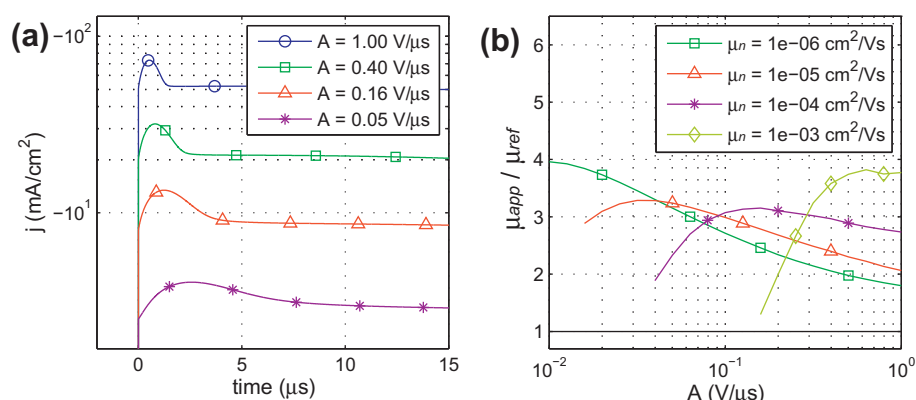


Fig. 5. (a) Simulated CELIV currents with varied voltage slope A ($\mu_n = 1 \times 10^{-4} \text{ cm}^2/\text{Vs}$, $\mu_p = 0.01 \cdot \mu_n$). (b) Apparent mobilities μ_{app} relative to the reference mobility μ_{ref} plotted versus the voltage slope A .

4.3. Influence of the voltage slope

In a next step we study the influence of the voltage slope on the CELIV results. The voltage slope is one of the parameters used in the analytical formula (Eq. (1)) to calculate the mobility. Ideally, the calculated mobilities do not depend on the voltage slope A that was used in the experiment. Fig. 5a shows CELIV currents with different voltage slopes. The current offset due to the displacement current is proportional to the voltage slope and follows $j = \frac{A}{d} \cdot \epsilon \cdot \epsilon_r$ where A is the voltage slope and d is the thickness. The current peak shifts to shorter times with higher voltage slope.

In Fig. 5b the relative apparent mobility is shown for varied voltage slopes. Using a low voltage slope for devices with a high mobility does not lead to reasonable CELIV currents. Therefore the apparent mobilities are only plotted in a specific range. For all the reference mobilities the apparent mobilities vary significantly with different voltage slopes. This variation can be up to a factor of 3. It has been proposed to obtain the electric field dependence of mobilities with CELIV by varying the voltage slope (Mozer et al., 2005.). This implies that a higher voltage slope leads to a higher electric field in the device. Therefore the variation of the extracted mobility was attributed to an electric field dependency of the mobility. With Fig. 5b we show that the extracted mobility is not constant with varied voltage slope even if constant mobilities are assumed.

Using CELIV to determine the field dependence of the mobilities is therefore not reasonable.

CELIV experiments on different devices should be done with the same voltage slope in order to get comparable results.

4.4. Numerical parameter extraction

Now we use our numerical model to fit measured CELIV current transients. The device structure and the measurement set-up are described in chapter Section 2. In a first step the series-resistance R_s and the relative

permittivity ϵ_r is determined. CELIV currents for several voltage slopes are measured in the dark. With the displacement offset j_0 the relative permittivity can be calculated as

$$\epsilon_r = \frac{j_0 \cdot d}{A \cdot \epsilon_0} \quad (10)$$

where A is the voltage slope and d is the thickness of the active layer. On the basis of the current slope immediately after the start of the voltage ramp it is possible to determine the total series resistance. It can be shown that R_s satisfies

$$R_s = \frac{A}{I_s} \quad (11)$$

where A is the voltage slope and $I_s = \left. \frac{dj}{dt} \right|_{t=0}$ is the initial current slope.

In order to keep the amount of unknown parameters low we use a simple model with constant mobilities and no traps. The barriers at the electrodes are assumed to be 0.3 eV. The height of the barrier has only a small influence on the CELIV current. There are 5 unknown parameters of this model namely the photon-to-charge generation efficiency G_{opt} , the electron mobility μ_n , the hole mobility μ_p , the Langevin recombination efficiency η and the built-in voltage V_{bi} . The transient current of one single CELIV experiment can exactly be reproduced with several sets of parameters. To obtain a unique set of parameters the simulation is fitted to multiple CELIV transients with varied voltage slope and the transient photo-current response (response to a light pulse).

The cell is illuminated and a voltage of 0.6 V is applied in the simulation as in the experiment. For each simulation the built-in voltage V_{bi} is adjusted such that no current flows at the beginning. This is necessary because a variation in the mobilities causes a changed current with a given built-in voltage and applied voltage. At 0 μs the illumination is turned off and the voltage ramp starts.

The fast carrier mobility mainly defines the temporal position of the CELIV-peak whereas the slow carrier mobility defines the tail of the current overshoot. Charge generation efficiency G_{opt} and the recombination efficiency

η have an influence on how many free charge carriers are inside the layer before the voltage ramp starts and therefore define the amplitude of the current overshoot when these charge carriers are extracted. The steady-state current of the pulsed experiment is defined by the charge generation efficiency, the recombination rate and the slow carrier mobility. The shape of the tail after illumination turn off is strongly influenced by the mobility ratio.

Using a very low intensity pulse (not shown) only few charge carriers are inside the bulk and recombination is negligible. In this case only the generation efficiency and the slow carrier mobility define the photo-current.

Fig. 6a shows the measured CELIV currents with different voltage slopes and the corresponding simulations. For all slopes the same set of parameters is used. The transient currents can in general be reproduced with the simple drift-diffusion model using constant mobilities.

At very high voltage slopes ($A = 2\text{ V/s}$) the current overshoot disappears. The simulation is overestimating the current in this case whereas in the case of low voltage slopes ($A = 0.2\text{ V/s}$) the current is slightly underestimated. A possible explanation is the electric field dependence of the mobilities. A higher mobility reduces the current peak because recombination is enhanced. Using the Poole–Frenkel model to describe the field dependence of the mobilities ($\mu(E) = \mu_0 \cdot e^{\gamma \sqrt{|E(x,t)|}}$) did not lead to better results in this study. The deviation could also be caused by traps if trapping and detrapping is field dependent. A further reason for this deviation may be related to charge transfer excitons (CT-exciton) whose dissociation is believed to be field dependent.

In Fig. 6b the photo-current response to a light pulse is shown. For the simulation the same set of parameters is used as for the CELIV simulation in Fig. 6a. The raise and the fall of the photo-current transients (Fig. 6b) show a slight deviation. This can be caused by trapping and releasing charge carriers that is not considered in this simulation. An influence of a field dependence of the mobility is also possible since with the given series-resistance on the sample a voltage drop of 0.3 V occurs.

Table 2
Simulation parameter used for the numerical fit in Fig. 6.

Material	Electron mobility	μ_n	$9 \times 10^{-4}\text{ cm}^2/\text{V s}$
	Hole mobility	μ_p	$1.3 \times 10^{-4}\text{ cm}^2/\text{V s}$
	(Mobility ratio)	ratio	0.14
	Relative permittivity	ϵ_r	5.13
	Langevin recombination efficiency	η	0.35
Device	Injection barriers	E_B	0.3 eV
	Built-in voltage	V_{bi}	0.82 V
Measurement set-up	Series resistance CELIV set-up	R_1	230 Ω
	Series resistance pulsed set-up	R_2	180 Ω
	Illumination time	t_{ill}	7 μs
	Delay time	t_{del}	0 μs
	Voltage offset	V_0	0.6 V

The simulation parameters used to reproduce the measurements are listed in Table 2. The resistance R_1 is the total series resistance of the CELIV set-up consisting of ITO-resistance (170 Ω), shunt resistance (10 Ω) and internal resistance of the waveform-generator (50 Ω). The resistance R_2 is the total series resistance of the pulsed set-up consisting of ITO-resistance (170 Ω) and shunt resistance (10 Ω). The time t_{ill} is the duration of the light pulse in the CELIV experiment whereas the time t_{del} stands for the delay between light turn off and start of the voltage ramp. The voltage offset V_0 is applied during illumination in order to prevent an initial current before the beginning of the voltage ramp. The charge generation efficiency is not shown because it scales linearly with the light intensity and the absolute light intensity of the measurement set-up is not precisely known.

5. Summary

We used a numerical drift-diffusion model to analyse the accuracy of the frequently used formulas to analyse CELIV

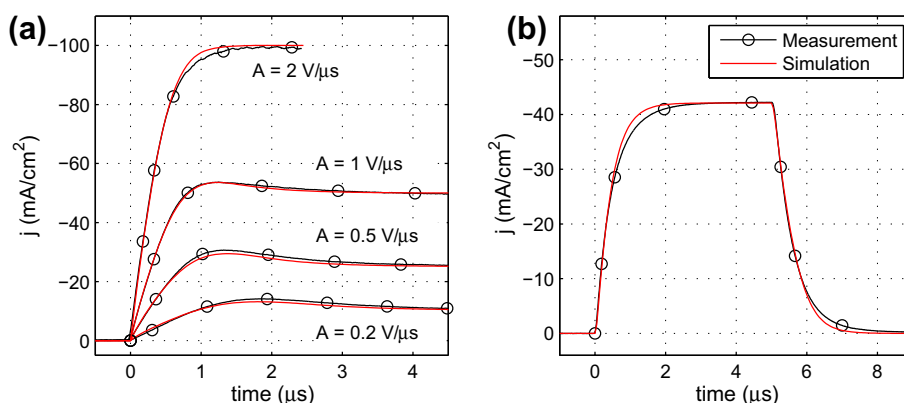


Fig. 6. (a) Measurement and simulation of transient CELIV currents for different voltage slopes. (b) Measurement and simulation of the transient photo-current as response to a 5 μs light pulse at 0 V applied voltage. Device structure in Table 1. Simulation parameters in Table 2.

experiments. We showed that the RC-time of the measurement set-up has a significant influence on the extracted mobilities. For thin cells ($d < 200$ nm) this is an important issue because thin films have a high capacitance. If the RC-time is high and cannot be reduced we recommend to use numerical simulation for parameter extraction with consideration of the series resistance.

In case of negligible RC-effects it has been shown that the analytical formulas are suitable to get the order of magnitude of the mobility but not an exact value.

Furthermore we showed that the determination of the field dependence of mobilities by a variation of the voltage slope A is not feasible because the extracted mobilities are not stable with a changing slope.

By fitting the numerical model to several CELIV currents and to transient photo-currents as response to a light pulse, we showed that not only the fast carrier mobility can be determined but also the slow carrier mobility, the generation- and the recombination efficiency. Thus a parameter set has been derived that successfully describes both types of experiments.

Trapping of electrons and holes was not considered in this study and could be added in a further step to analyse ageing mechanisms in organic solar cells, for instance.

Acknowledgments

The organic semiconductors, cyclo-voltammetry and ellipsometry measurements were kindly provided by Mathieu Turbiez and colleagues at BASF in Basel. We thank Ton

Offermans and colleagues at CSEM Basel for the fabrication of the organic solar cells. The authors gratefully acknowledge financial support from the Swiss Federal Office of Energy for funding the POLYMOL project called *Apollo*.

References

- Bange, S., Schubert, M., Neher, D., 2010. Phys. Rev. B 81, 035209.
- Häusermann, R., Knapp, E., Moos, M., Reinke, N.A., Flatz, T., Ruhstaller, B., 2009. J. Appl. Phys. 106, 104507.
- Hwang, I., McNeill, C.R., Greenham, N.C., 2009. J. Appl. Phys. 106, 094506.
- Juska, G., Arlauskas, K., Viliunas, M., Kocka, J., 2000. Phys. Rev. Lett. 84, 4946.
- Juska, G., Viliunas, M., Arlauskas, K., Nekrases, N., Wyrsh, N., Feitknecht, L., 2001. J. Appl. Phys. 89, 4971.
- Lorrmann, J., Badada, B.H., Ingans, O., Dyakonov, V., Deibel, C., 2010. Mater. Sci., 1006.4394v1.
- Mark, P., Lampert, M.A., 1970. Current Injection in Solids. Academic Press, New York.
- Mort, J., Pai, D.M., 1976. Photoconductivity and Related Phenomena. Elsevier, New York.
- Mozer, A.J., Sariciftci, N.S., Lutsen, L., Vanderzande, D., Österbacka, R., Westerling, M., Juska, G., 2005. Appl. Phys. Lett. 86, 112104.
- Mozer, A.J., Dennler, G., Sariciftci, N.S., Westerling, M., Pivrikas, A., Österbacka, R., Juska, G., 2005. Phys. Rev. Lett. B 72, 035217.
- Neukom, M.T., Reinke, N.A., Brossi, K.A., Ruhstaller, B., 2010. Proc. SPIE 7722, 77220V.
- Offermans, T., Schleuniger, J., Nisato, G., 2010. LOPE-C, 99–102. Semiconducting thin film optics simulator (SETFOS) by Fluxim, A.G., Switzerland. <www.fluxim.com>.
- Solamer achieves 8.13 percent OPV efficiency, PV Magazine. <www.pv-magazine.com> (28.07.10).